The mechanical stress–strain properties of single electrospun collagen type I nanofibers

C.R. Carlisle, C. Coulais [1], M. Guthold *

Department of Physics, 7507 Reynolda Station, Wake Forest University, Winston-Salem, NC 27109, USA

ABSTRACT

Knowledge of the mechanical properties of electrospun fibers is important for their successful application in tissue engineering, material composites, filtration and drug delivery. In particular, electrospun collagen has great potential for biomedical applications due to its biocompatibility and promotion of cell growth and adhesion. Using a combined atomic force microscopy (AFM)/optical microscopy technique, the single fiber mechanical properties of dry, electrospun collagen type I were determined. The fibers were electrospun from a 80 mg ml^{-1} collagen solution in 1,1,1,3,3,3-hexafluoro-2-propanol and collected on a striated surface suitable for lateral force manipulation by AFM. The small strain modulus, calculated from three-point bending analysis, was 2.82 GPa. The modulus showed significant softening as the strain increased. The average extensibility of the fibers was 33% of their initial length, and the average maximum stress (rupture stress) was 25 MPa. The fibers displayed significant energy loss and permanent deformations above 2% strain.

© 2010 Acta Materialia Inc. Published by Elsevier Ltd. All rights reserved.

1. Introduction

Collagen type I is a common element of the extracellular matrix (ECM) and plays an important structural role in the body, providing strength and support to the aorta, skin, bones, ligaments and tendons, to name a few [1–3]. The fundamental unit of collagen type I is composed of a triple helix consisting of three polypeptide chains, two α1(I) collagen chains and one α2(I) collagen chain [4], held together by hydrogen bonds and disulfide bonds. It has a length of ∼300 nm and a diameter of 1.5 nm. These collagen triple helices aggregate to form collagen fibrils with an average diameter between 50 and 200 nm and quarter stagger molecular arrangement resulting in a 67-nm banding pattern or D-periodicity. The banding pattern can be seen under high resolution transmission electron microscopy [5]. Mechanical support, helping to resist tissue strain, is provided to adjacent collagen molecules by enzyme-mediated cross-linking [6]. Natural collagen structures show a range of biomechanical properties from those of bone, with a modulus of 17.2 GPa [7], to that of skin, with a modulus of 4 GPa [2].

Aside from naturally formed collagen fibers, collagen fibers can also be produced through the process of electrostatic spinning. In this procedure, fibers are formed from a highly concentrated polymer in a volatile solvent. The solution is charged to a high voltage and pumped from a syringe towards a grounded collector plate.

The electric field, between the syringe and the collector, and the surface tension apply opposing forces to the liquid as it is expelled from the needle. When the force of the electric field exceeds the surface tension, a Taylor cone is formed, and the charged, volatile solution is expelled from the tip in a very small stream [8]. As the jet approaches the grounding plate, instabilities in the jet lead to whipping, bending and thinning of the jet [9,10]; ultimately the diameter of the fiber is lowered to a value between 10 nm and 10 μm. Experimental parameters, such as working distance, polymer concentration, voltage and flow rate, can be altered to produce fibers of desired diameters and porosity [11].

The ease with which electrospun fibers can be produced makes them an ideal candidate for material composites and biomedical engineering applications, such as tissue engineering scaffolds, wound dressings, coatings or drug delivery vehicles [11]. The diameter of electrospun fibers mimics that of the natural ECM and other biological fibers. Electrospun collagen, in particular, has great potential in scaffold engineering, because biomechanical structures formed from collagen have been shown to supply a substrate for cell adhesion, improving cell growth and differentiation [12], while the helicity and rigidity of the collagen molecule supply strength [13]. Scaffolds constructed from collagen blends have been studied *in vitro* for vascular graft applications [14] and have shown potential as a treatment for skeletal muscle tissue defects [15].

The mechanical properties of biomedically engineered devices are very important to their function. First, the mechanical properties of the substrate affect cell differentiation [16]. Second, the

* Corresponding author. Tel.: +1 336 758 4977; fax: +1 336 758 6142.
E-mail address: gutholdm@wfu.edu (M. Guthold).
[1] Present address: SPEC, CEA Saclay, 91191 Gif sur Yvette Cédex, France.

scaffold must have similar properties to the natural tissue it is replacing so that it can perform the function of the tissue. Finally, scaffolds must have the mechanical stability to handle manipulation by the physician during implantation as well as support tissue regeneration and structure degradation [17].

Characteristics such as orientation, density and mechanical properties of the constituent fibers determine whether the scaffold will have the desired mechanical properties. Techniques using rotating and split electrode collectors have been used to orient fibers [18–21]; and tests on oriented electrospun mats have shown that fiber orientation affects collagen matrix properties [22]. This study examines the properties of the constituent of the matrix, the individual electrospun fibers. Recently, the bending modulus of individual electrospun collagen type I fibers was determined [23]. The present study expands on this knowledge of the mechanical properties of individual electrospun collagen type I fibers by determining the strain softening behavior, extensibility, maximum stress, energy loss and deformation characteristics using lateral force atomic force microscopy (AFM).

2. Materials and methods

2.1. Substrate preparation

The substrate was prepared using a soft lithography and MIMIC (micromoulding in capillaries) technique [24]. A SU-8-silicon master grid with channels 12 μm wide and 6 μm deep and ridges 8 μm wide was used to create a polydimethylsiloxane (PDMS) stamp by pouring dimethylsiloxane plus catalyst (Sylgard, Dow Corning Corp., Midland, MI) onto the grid and curing the PDMS at 70 °C for 1 h. A striated surface was formed on the top of a 60 × 24-mm, #1.5, microscope cover by pressing the PDMS stamp into a 10 μl drop of Norland Optical Adhesive-81 (NOA-81, Norland Products, Cranbury, NJ). The optical adhesive was cured for 70 s, with UV light (365 nm) (UVP 3UV transilluminator, Upland, CA) (Fig. 1A).

2.2. Electrospinning

A polymer solution, consisting of collagen type I, acid soluble from calf skin at 80 mg ml^{-1} (Elastin Products Company, Owensville, MO) and 1,1,1,3,3,3-hexafluoro-2-propanol (HFP) was prepared. The solution was poured into a 1-ml volume, 4-mm diameter syringe. The syringe was fitted with a 23 × ¾-gauge butterfly and tubing infusion set needle and was placed in the syringe pump (NE-1000 Programmable Syringe Pump, New Era Pump System, Inc., Wantagh, NY) and dispensed at a rate of 2 ml h^{-1}. A voltage of 18 kV was applied to the syringe needle. The striated substrate was grounded with an alligator clip and placed at a distance of 25 cm from the needle.

2.3. Combined AFM/inverted optical microscopy

The mechanical manipulations were performed as previously reported [25]. Briefly, a combined atomic force microscope (Topometrix Explorer, Veeco Instruments, Woodbury, NY) and optical microscope (Zeiss Axiovert 200, Göttingen, Germany) instrument was used to manipulate and observe fiber manipulation [26,27]. The dual microscopy system is set up so that the AFM rests on a custom-made stage on top of the inverted microscope (Fig. 1B). The design allows for independent movement of the microscope objective, AFM cantilever and sample. For schematic see Ref. [25]. Light was provided to the sample from the cantilever illumination bulb on the underside of the AFM. A Hamamatsu EM-CCD C9100 Camera (Hamamatsu Photonics KK, Japan) and IPlab software (Scanalytics, Fairfax, VA) were used to collect and analyze the bright field microscopy images and movies.

2.4. Fiber manipulations and force calculations

Fiber manipulation and force acquisition was obtained as previously reported [25]. Silicon cantilevers with a rectangular cross-section were used for AFM imaging, fiber manipulation and force acquisition (NSC12 without Al, force constant 14 N m^{-1}, length 90 μm, width 35 μm, tip height 15 μm; MikroMasch, Wilsonville, OR). Silicon cantilevers were used because of their commercial availability, large modulus ($E = 1.69 \times 10^{11}$ N m^{-2}) and, therefore, negligible compliance compared with the fiber deflections. The AFM cantilever was controlled by a nanoManipulator (3rd Tech, Chapel Hill, NC). The AFM tip was placed next to the fiber in the center of the grove. It was then moved into the fiber, stretching the fiber laterally (Fig. 1C). The typical pulling rate was ∼350 nm s^{-1}. Since the tip was located in the groove of the surface, frictional forces were eliminated. Stress–strain data were acquired by converting the left–right photodiode signal I_l, recorded by the nanoManipulator, into lateral force, $F_l = K_C \cdot I_l$. The conversion requires the lateral force conversion factor K_C, which can be determined from cantilever beam mechanics, $K_C = \frac{Ewt^3}{6l^2(h+t/2)} \cdot S_n$, where E, w, t, l and S_n are Young's modulus of silicon, 1.69×10^{11} N m^{-2}, the width, the thickness, the length and the normal sensor response of the cantilever, and h is the height of the tip. The length, width and height of the tip were determined using the optical microscope, and the thickness is calculated using the resonance frequency of the cantilever, $f = 0.276 \cdot \sqrt{\frac{Ewt^3}{\rho(\pi \cdot h^3 \cdot l^3 + 2.832 \cdot w \cdot t \cdot l^4)}}$, where $\rho = 2330$ kg m^{-3} is the density of silicon.

To convert force to stress ($\sigma = F/A$), the radius of the fiber was determined. Since the fiber diameters were often below the resolution limit of optical microscopy, the AFM was used in tapping mode to collect a topographical image of the manipulated fiber where it extended on top of the ridge. The diameter of the fibers was then determined from the z axis topographical data. The stress
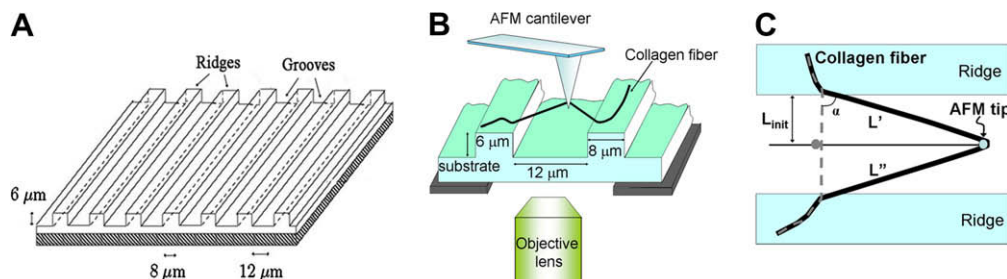

Fig. 1. (A) Schematic of the striated surface micromolded from optical glue. The ridges are 8 μm wide by 6 μm high and the grooves are 12 μm wide. (B) Schematic of the experimental setup. The AFM tip is used to stretch fibers that are suspended over the ridges in a striated substrate. (C) Representation of a stretched fiber across the ridge and well-striated surface. The final length of the fiber $L' + L''$ can be calculated from knowledge of its initial length L_{init} and the distance the AFM tip traveled, s. The calculated values can be compared directly with values measured from the optical image. (Figure adapted from Ref. [25]).

was calculated assuming a constant fiber radius; this is termed the engineering stress.

3. Results

Fibers were electrospun from a solution of 80 mg ml^{-1} collagen type I dissolved in HFP and were collected on cover glass stamped with a striated surface. The striated surface had grooves 12 μm wide and 6 μm deep and ridges 8 μm wide. The collected fibers had a uniform appearance and were randomly oriented on the surface (Fig. 2). The average fiber radius as determined by AFM topography was 302 ± 126 nm. In addition to investigating fibers in ambient conditions, an attempt was also made to examine fibers that were rehydrated in aqueous buffer. However, as previously reported, the electrospun collagen fibers were partially soluble in buffer if they were not crosslinked [28,29]. Therefore, due to loss of fiber integrity, it was not possible to take meaningful data on the hydrated fibers in buffer.

The mechanical properties of the electrospun collagen type I fibers were tested using a combined AFM and inverted optical microscope system. Fibers oriented perpendicularly to the ridge were chosen for manipulation, because they provided an easy to analyze geometry (see Section 2). The fibers were stretched parallel to the ridges using the AFM tip, and stress–strain curves were obtained (Fig. 3A–D). Fig. 3E shows a typical electrospun collagen type I stress–strain curve. The slope of the stress–strain curve characterizes the stiffness of the material. The stress–strain curves of the electrospun collagen fibers showed considerable strain softening, i.e., a decrease in modulus (stiffness) as the strain increases. Because of the strain softening, the commonly used three-point bending model (with clamped ends) was chosen to calculate the small strain bending modulus, $E = \frac{F \cdot l^3}{48 \cdot x \cdot \pi \cdot r^4}$, where F is the force, l is the length of the fiber, x is the displacement, and r is the radius. The three-point bending modulus was determined for displacements up to 200 nm ($\varepsilon \leqslant 0.056\%$). The average three-point bending modulus of electrospun collagen type I fibers was 2.8 ± 0.4 GPa (value ± standard error; $n = 32$). The modulus of the fibers had a strong dependence on radius; as the radius of the fibers increased, the modulus decreased (Fig. 4A). The radii of the fibers tested ranged from 160 nm to 783 nm. The value of the modulus and modulus dependence on radius agrees with previously published data [23].
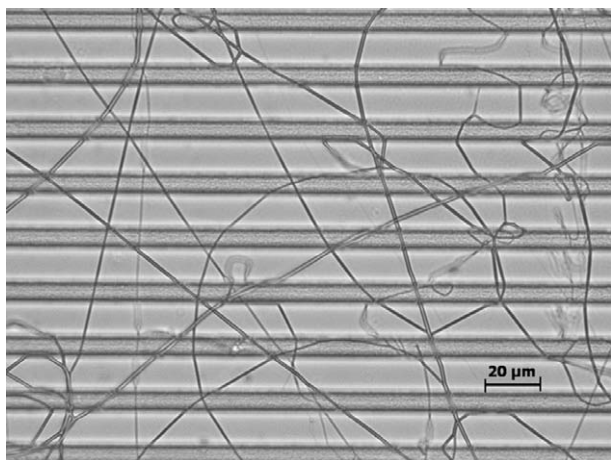

Fig. 2. Optical microscope image of the electrospun collagen type I sample. The ridges are visible as darker gray horizontal stripes 8 μm wide and are spaced by lighter gray 12-μm grooves. The electrospun fibers are randomly oriented on the surface. Fibers aligned perpendicular to the ridges are selected for manipulation.

The extensibility, or strain at which the fiber ruptures, was determined via the same fiber manipulations used to determine the modulus (Fig. 3E). The extensibility of 24 fibers was measured, and the average extensibility of electrospun collagen type I fibers was 33 ± 3%. The extensibility of the fibers showed no dependence on fiber radius in the tested range 160–783 nm.

The next property analyzed was the maximum stress or peak stress. The maximum stress is the highest stress value reached before the fiber ruptures (Fig. 3E). In all manipulations, the softening of the fiber modulus led to a plateau in the stress applied to the fiber. As the strain increased from zero to ∼12% strain, the stress increased. At 12% strain, the stress applied to the fiber reached a plateau, where it remained until the fiber ruptured. The maximum stress therefore occurred at 12% strain and, at strains above 12%, the fiber remained at the maximum stress until the fiber ruptured. The maximum stress for 15 fibers was measured, and the average maximum stress was 25 ± 3 MPa. The maximum stress varied with fiber radius, similar to the modulus, as the radius increased, the maximum stress decreased (Fig. 4B). In calculating the peak stress, the radius prior to manipulation was used; thus, engineering stress was used to calculate the peak stress. While this assumption may not be accurate to describe the behavior of the fiber during manipulation, Poisson's ratio of electrospun collagen is not known and therefore cannot be used in the calculation. The engineering stress gives a lower boundary to the value of the peak stress. Another method of stress calculation used in the absence of the Poisson ratio of the material is to assume that the fiber maintains a constant volume during manipulation. The engineering stress can be converted to stress calculated for a constant volume using the equation, $\sigma = \frac{F}{A}(\varepsilon + 1)$, where F is the force, A is the cross-sectional area of the fiber before manipulation, σ is the stress, and ε is the strain.

Next, stress–strain data were taken to probe energy storage and dissipation. In viscoelastic material, a portion of the energy used to stretch the material is stored elastically, while the rest of the energy is lost or dissipated to the surroundings through viscous processes. The energy dissipated or lost is proportional to the area between the forward and backward curve of the stress–strain plot (Fig. 5A). The percentage of the input energy lost during a stretch cycle was strongly dependent on the maximum strain of the cycle. At low strains, smaller percentages of energy loss occurred, and the material behavior was mostly elastic. However, at higher strains significant energy loss was seen. The energy loss per cycle increased linearly with increasing strain up to a strain of 12%, at which point the energy loss saturated at 80% of the input energy. In other words, at strains above 12%, 80% of the energy required to stretch the fiber was not recovered as the fiber returned to the starting position. At low strain, the energy loss followed an approximately linear increase from 0% energy loss at 0% strain to 80% energy loss at 12% strain (Fig. 5B).

When electrospun collagen type I fibers were stretched and returned to their initial position, permanent deformation was detectable both visibly and through the stress–strain data. Visibly, when the force stretching the fibers is released, they do not return to their original shape; instead, the fibers appear less taught and permanently deformed between the ridges. The stress–strain curve shows the permanent deformation in that the stress applied to the fiber, or the stress applied to the cantilever by the fiber, returns to zero before the fiber returns to its initial zero-strain position. The black curve in Fig. 5C shows a manipulation of a fiber. On the return manipulation, the stress returns to zero before the strain is zero indicating deformation in the fiber. As shown in Fig 5C, electrospun collagen type 1 fibers also show significant hysteresis. The slope of the stress–strain curve for a second manipulation is less than that of the first manipulation (Fig. 5C).
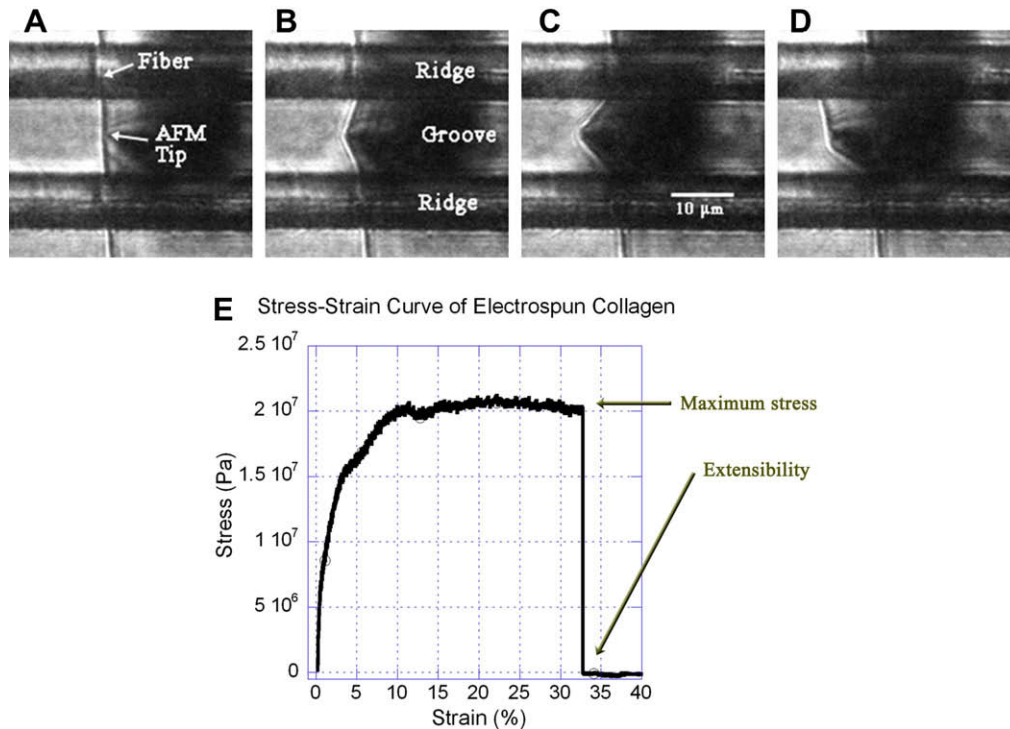
Fig. 3. (A–D) Movie frames from an electrospun collagen fiber manipulation. The AFM cantilever is visible as a large, vertical shadow covering the right side of the image. The tip of the AFM can be seen to the left of the cantilever shadow due to optical parallax and the dark horizontal lines are the ridges of the patterned surface. (D) The fiber has broken at the top ridge. (E) Typical stress–strain curve acquired during a fiber manipulation. The stress increases as the strain increases, but the rate at which the stress increases changes with strain and the fiber displays modulus softening with increasing strain. At the point when the fiber breaks, the stress drops back to zero. The strain value at which the fiber ruptures is the fiber's extensibility. This fiber has an extensibility of 33%. The maximum stress can also be obtained from the graph; this fiber has a maximum stress of 21 MPa.

4. Discussion

A combined atomic force/optical microscopy technique was used to probe the mechanical properties of nanometer-sized, dry, electrospun collagen type I fibers through the collection of various stress–strain measurements. The extraction of mechanical properties through AFM lateral force manipulation has been used previously for measurements on natural fibrin fibers [30] and electrospun fibringen fibers in buffer [25]. Errors in the data acquired by the combined microscopy technique result from force and radius measurements, obtained by the AFM. The force measurements are calibrated against the cantilever beam method and the glass fiber method (see Ref. [31]), while the radius measurements are calibrated against a grid of known dimensions. The error in the force measurements is estimated to be ~30%, and the error in the radius measurement ~20%. While the errors in these measurements are larger than those of other nanomanipulation methods, such as the scanning mode bending test with 12% error in the force measurement [32–34], this type of lateral force AFM data has shown agreement with various methods of nanomanipulation [23,30,35]. In addition, the combined AFM/optical microscope measurements have the advantage that the fiber is visualized throughout the entire manipulation process, and that it allows for very large extensions, up to fiber failure.

Applying the combined microscopy technique to the electrospun collagen fibers, it was found that the fibers show clear viscoelastic behavior. The three-point bending modulus for deformations <200 nm ($\varepsilon \leqslant 0.056\%$) ranges from 0.2 to 8.0 GPa with an average of 2.8 GPa. This is in agreement with previously published data by Yang et al. on the modulus of individual electrospun collagen fibers determined by scanning mode bending [23]. Yang also observed a decrease in the modulus of the fiber with increasing

radius, which was also clearly evident from the present data [23]. The relationship between radius and modulus has also been seen in electrospun carbon nanofibers, where heterogeneities in longitudinal and cross-sectional area were deemed responsible for the complex association between radius and modulus [36]. Internal voids or molecular density may vary with respect to electrospun fiber size, producing a larger fiber that is less dense or more porous than smaller fibers. This, in turn, would affect the modulus so that the larger fibers had a lower modulus than smaller fibers. However, Pai et al. [37] found that, while the void size varied with fiber radius, the void to volume fraction remained relatively constant among electrospun fibers. Another explanation for the observed modulus dependence on radius is greater orientation (alignment) in smaller fibers. Lim et al. [38] explained that the distribution of fiber diameters is formed from the random whipping of the jet as it approaches the collector plate. Sections of the jet become thinner, with greater molecular orientation and crystalline order as they undergo greater amounts of bending, elongation and solvent evaporation before reaching the surface. Lim et al. also demonstrated that the thinner, more crystalline fibers displayed greater stiffness and strength. It is likely that varying molecular orientation with fiber radius is also responsible for the modulus dependence on radius seen in electrospun collagen fibers.

One advantage of lateral force AFM over scanning mode bending and optical tweezing is that it allows for a large range of manipulation of individual electrospun fiber, including fiber failure. Continuous manipulation of the fibers until failure showed severe strain softening of the electrospun collagen type I fibers. The modulus of the fibers decreased drastically as the strain increased. At a strain of ~12%, the modulus decreased to nearly zero and remained at that value until fiber rupture at an average strain of 33%. This plateau in the stress–strain curve can be attributed to plastic defor-

A

Modulus dependence on radius

B

Maximum stress versus radius
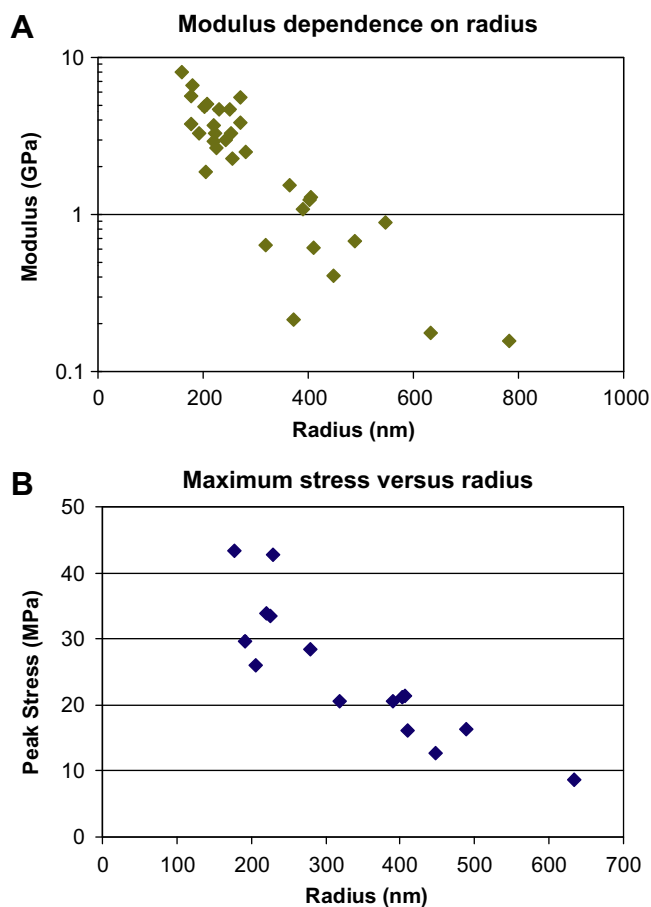
Fig. 4. (A) Plot of modulus vs radius. The modulus decreases with increasing radius. (B) Plot of maximum stress vs radius. The maximum stress decreases with increasing fiber radius.

mation of the fibers. Data on micron-sized electrospun collagen fibers and mats also display similar significant strain softening [39]. At 12% strain, a similar trend was seen in the energy loss data. The energy loss in a manipulation cycle increased linearly from 0% energy loss at 0% strain to 80% energy loss at 12% strain; for strains >12%, the energy loss remained at 80% of the input energy.

It appears, however, that plastic deformation begins within the fibers before the modulus decreases to zero. The energy loss data suggest that electrospun collagen fibers undergo plastic deformation, beginning as low as 1% strain, and visible data suggest that permanent deformation occurs above 2% strain; that is, fibers undergoing manipulations >2% strain do not return to their original shape once they have been manipulated. Aside from single manipulation deformations, electrospun collagen also shows hysteresis, or memory of previous manipulations. The initial manipulation of the fiber alters its properties; a second manipulation to a strain of equal or lesser value gives altered stress–strain behavior. However, subsequent strains, such as third or fourth manipulations, will have identical stress–strain behavior as the second manipulation. This suggests that, in applications involving cyclic stress on electrospun collagen, the original response of the material as well as the material hysteresis should be considered. Preparing electrospun collagen for use may require an initial manipulation of the material to obtain reproducible mechanical properties.

Individual electrospun collagen type I fibers can be stretched to 1.33 times their initial length before rupturing. In comparison with wet electrospun fibrinogen fiber, another biocompatible protein with an extensibility of 2.3 × their original length [25], collagen

is less extensible. However, the maximum stress of both dry electrospun collagen and wet fibrinogen is on the order of 20–30 MPa. It is important to consider fiber radius when considering maximum stress, since the maximum stress displayed an inverse dependence on radius. Extensibility, however, did not depend on radius.

Previously, Matthews et al. [40] showed that the average modulus for longitudinally oriented electrospun collagen mats is 52.3 ± 5.2 MPa, with a peak stress of 1.5 ± 0.2 MPa. From these reports it is evident that the initial modulus and peak stress for individual fibers differ from the properties of the mats. The difference in modulus between mats and individual fibers is most likely due to the greater architectural complexity of the electrospun mats. For example, fiber orientation plays a major role in the mechanical behavior of the mats, and it directly influences the modulus and peak stress of the mat [40]. A second element of complexity is the effect of fiber radius on the modulus and peak stress of the mat. One simple way to change the modulus or peak stress of an electrospun mat might be to decrease or increase the average fiber radius. Therefore, collagen mats with a range of mechanical properties could be fabricated by controlling fiber diameter through solvent concentration and other spinning factors [41,42], as well as controlling the orientation of the fibers.

In addition to comparison with electrospun collagen type I mats and electrospun fibrinogen, the individual fibers can be compared with their natural counterparts. Natural collagen type I fibers from rat tail have a modulus between 5 and 11.5 GPa, and collagen type I fibrils from bovine Achilles tendon have a dry bending modulus between 1 and 4 GPa [32,43]. These values are similar to the initial modulus of 2.8 GPa recorded for individual electrospun collagen fibers. As mentioned previously, in biomedical engineering applications, the mechanical properties of a scaffold have a large effect on cell proliferation, and therefore similarity between native fiber and electrospun fibers is beneficial to biomedical engineering [16]. However, electrospun fibers cannot be directly compared with native fibers. Electrospun fibers are produced in HFP, a highly volatile buffer. HFP and similar fluorinated hydrocarbon buffers have been shown to promote α-helix formation [44]. Circular dichroism spectra of electrospun collagen fibers have shown that 45% of their proline helical content of collagen is denatured in HFP [45], and therefore the individual monomers composing electrospun fibers are different from native collagen monomers. It has also been argued that collagen denatures into gelatin in fluorinated solvents such as HFP [29]. However, tensile tests on collagen and gelatin mats have revealed different tensile moduli for the two molecules, suggesting that, while collagen is denatured in HFP, it does display different behavior from gelatin electrospun in HFP [46]. It should also be mentioned that electrospun collagen fibers may have many more uses than for tissue engineering. The dried, uncrosslinked fibrin fibers may be especially useful in applications were the scaffolds needs to dissolve after a while, such as wound dressings, coatings or drug delivery vehicles [11]. Despite the difference in the protein structure between native and electrospun collagen molecules, their fibers show somewhat similar mechanical behavior compared with other biological fibers, as they are both relatively stiff and not very extensible [47].

The use of individual fiber properties in matrix modeling has been shown through combined microscopic and macroscopic modeling [48–50]. In these studies, whole matrix properties are modeled, starting at the individual fiber and including fiber orientation. From these models, ideal scaffolds could be designed with the knowledge and control of individual fiber properties and fiber orientation. Generally, three elements are needed to explain and design matrix properties [51,52]: (1) the properties of the individual constituents; (2) the properties of fiber interactions or branch points of the network; and (3) the overall network architecture. Developments in controlling electrospun fiber orientation
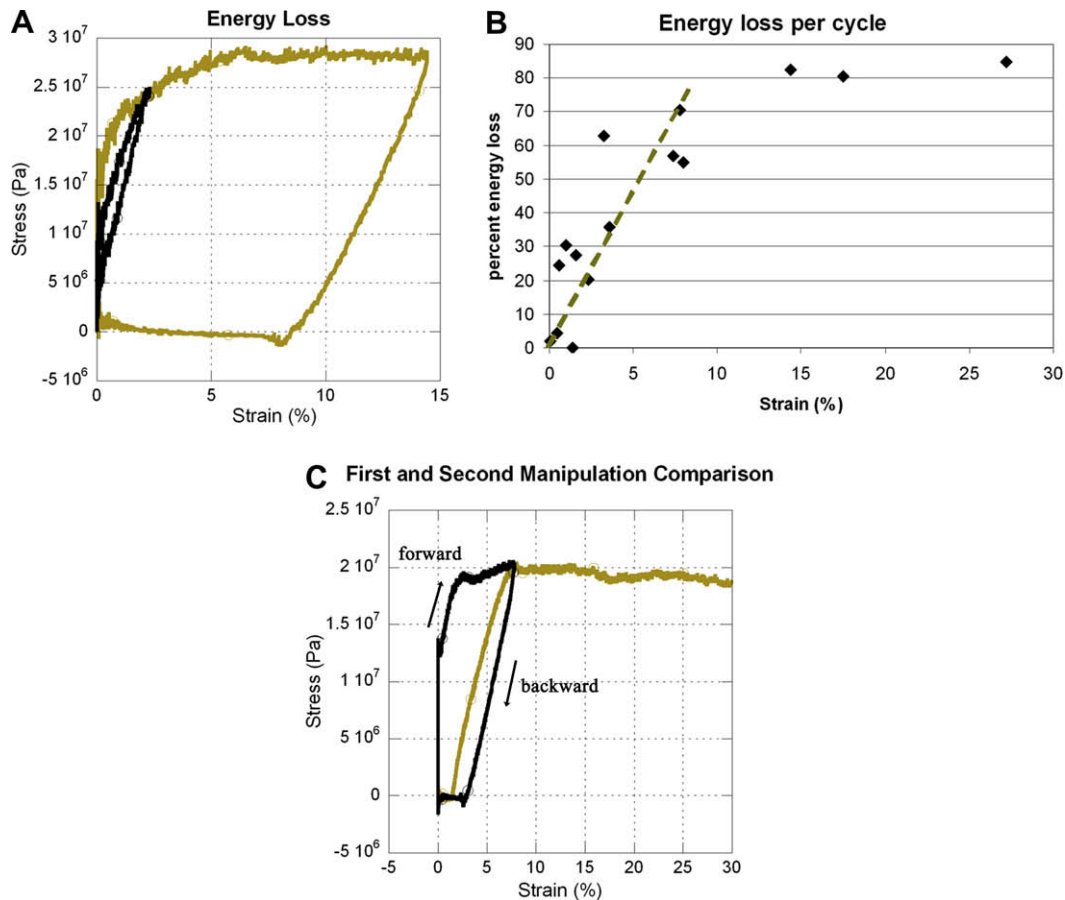
Fig. 5. (A) Stress–strain curves depicting energy loss during a stretch cycle. The forward pull requires more force and therefore has a higher stress than the backward pull. The fiber indicated by the black curve was pulled to a strain of 2.3% and showed 20% energy loss; the gold fiber was pulled to a strain of 14.4%, and the fiber had an energy loss of 82.5%. (B) Graph of energy loss vs strain. The gold dashed line shows the slope of the increasing energy loss as strain increases. At 12% strain, the energy loss plateaus at 80%. (C) Stress–strain curve of two consecutive manipulations of the same fiber. The first manipulation is shown in black. The stress required to stretch the fiber during the first manipulation differs from the stress required for the second manipulation, shown in gold.

show promise for control over network architecture, fiber branching is minimal in electrospinning, fiber interactions are based on friction between overlaying fibers, and here the individual fiber properties are described.

The use of electrospun protein fibers for medical application is inspired by the properties and components of the ECM itself. By mimicking the size and mechanical properties of the ECM, it is thought one may achieve good cellular adhesion and materials properties desired for tissue engineering. However, the application of electrospun fibers does not stop with tissue engineering; uses in drug delivery, and dental composites have also gained recognition [53–55]. Through studies on the mechanical properties and response of single fibers, insight is gained into improvements that could be made in fiber selection and formation for materials use.

5. Conclusion

In summary, the combined microscopy technique has been shown to be a good tool for extracting the mechanical properties of individual electrospun nanofibers. The mechanical properties of individual electrospun collagen type I fibers were determined, and it was shown that electrospun collagen undergoes severe strain softening, and the modulus and peak stress of the individual electrospun collagen type I fibers have a dependence on radius. It is believed that determining the properties of individual electrospun fibers will help in understanding the properties of electrospun fiber mats from the ground up, potentially leading to the ability to

assemble electrospun matrices with the desired mechanical strength, mechanical properties and biocompatibility for their intended function, whether medical or textile.

Appendix A. Figures with essential colour discrimination

Certain figures in this article, particularly Figs. 1 and 3–5, are difficult to interpret in black and white. The full colour images can be found in the on-line version, at doi: 10.1016/ j.actbio.2010.02.050.

References

[1] Dunn M, Silver F. Viscoelastic behavior of human connective tissues: relative contribution of viscous and elastic components. Connect Tissue Res 1983;12(1):59–70.
[2] Silver FH, Freeman JW, DeVore D. Viscoelastic properties of human skin and processed dermis. Skin Res Technol 2001;7(1):18–23.
[3] Silver FH. Biological materials: structure, mechanical properties and modeling of soft tissues. New York: New York University Press; 1987.

[4] Piez KA, Eigner EA, Lewis MS. The chromatographic separation and amino acid composition of the subunits of several collagens. Biochemistry 1963;2(1):58–66.

[5] Schmitt Francis O, Hall CE, Jakus Marie A. Electron microscope investigations of the structure of collagen. J Cell Comp Physiol 1942;20(1):11–33.

[6] Eyre DR, Paz MA, Gallop PM. Cross-linking in collagen and elastin. Annu Rev Biochem 1984;53:717–48.

[7] Reilly DT, Burstein AH. The mechanical properties of cortical bone. J Bone Joint Surg Am 1974;56(5):1001–22.

[8] Taylor G. Disintegration of water drops in an electric field. Proc R Soc Lond Ser A. Math Phys Sci 1964;280(1382):383–97.

[9] Rutledge GC, Fridrikh SV. Formation of fibers by electrospinning. Intersect Nanosci Mod Surf Anal Methodol 2007;59(14):1384–91.

[10] Shin YM et al. Electrospinning: a whipping fluid jet generates submicron polymer fibers. Appl Phys Lett 2001;78(8):1149–51.

[11] Huang Z-M et al. A review on polymer nanofibers by electrospinning and their applications in nanocomposites. Compos Sci Technol 2003;63(15):2223–53.

[12] Kleinman HK, Klebe RJ, Martin GR. Role of collagenous matrices in the adhesion and growth of cells. J Cell Biol 1981;88(3):473–85.

[13] Lodish H et al. Molecular cell biology. 4th ed. New York: W.H. Freeman; 2000.

[14] Sang Jin Lee JJY, Lim Grace J, Atala Anthony, Stitzel Joel. In vitro evaluation of electrospun nanofiber scaffolds for vascular graft application. J Biomed Mater Res A 2007;83A(4):999–1008.

[15] Choi JS CR et al. The influence of electrospun aligned poly([var epsilon]-caprolactone)/collagen nanofiber meshes on the formation of self-aligned skeletal muscle myotubes. Biomaterials 2008;29(19):2899–906.

[16] Engler AJ et al. Matrix elasticity directs stem cell lineage specification. Cell 2006;126(4):677–89.

[17] Li W-J et al. Electrospun nanofibrous structure: a novel scaffold for tissue engineering. J Biomed Mater Res 2002;60(4):613–21.

[18] Theron A, Zussman E, Yarin AL. Electrostatic field-assisted alignment of electrospun nanofibres. Nanotechnology 2001(3):384.

[19] Zussman E, Theron A, Yarin AL. Formation of nanofiber crossbars in electrospinning. Appl Phys Lett 2003;82(6).

[20] Wang HB et al. Creation of Highly aligned electrospun poly-l-lactic acid fibers for nerve regeneration applications. J Neural Eng 2009;6(1).

[21] Li D, Wang Y, Xia Y. Electrospinning nanofibers as uniaxially aligned arrays and layer-by-layer stacked films. Adv Mater 2004;16(4):361–6.

[22] Matthews JA et al. Electrospinning of collagen nanofibers. Biomacromolecules 2002;3(2):232–8.

[23] Yang L et al. Mechanical properties of single electrospun collagen type I fibers. Biomaterials 2007;29:955–62.

[24] Xia YN, Whitesides GM. Soft lithography. Angewandte Chem – Int Ed 1998;37(5):551–75.

[25] Carlisle CR et al. The mechanical properties of individual, electrospun fibrinogen fibers. Biomaterials 2009;30(6):1205–13.

[26] Liu W et al. The mechanical properties of individual, electrospun fibrinogen fibers. Science 2006;313:634.

[27] Peng L et al. A combined atomic force/fluorescence microscopy technique to select aptamers in a single cycle from a small pool of random oligonucleotides. Microsc Res Tech 2007;70:372–81.

[28] Buttafoco L et al. Electrospinning of collagen and elastin for tissue engineering applications. Biomaterials 2006;27(5):724–34.

[29] Zeugolis DI et al. Electro-spinning of pure collagen nano-fibres – just an expensive way to make gelatin? Biomaterials 2008;29(15):2293–305.

[30] Liu W et al. The mechanical properties of single fibrin fibers. J Thromb Haemost, 2010. doi:10.1111/j.1538-7836.2010.03745.x.

[31] Liu W, Bonin K, Guthold M. Easy and direct method for calibrating atomic force microscopy lateral force measurements. Rev Sci Instrum 2007;78(6):063707.

[32] Yang L et al. Mechanical properties of native and cross-linked type I collagen fibrils. Biophys J 2008;94(6):2204–11.

[33] Akihiro T et al. A method for determining the spring constant of cantilevers for atomic force microscopy. Meas Sci Technol 1996;2:179.

[34] Sattin BD, Pelling AE, Goh MC. DNA base pair resolution by single molecule force spectroscopy. Nucleic Acids Res 2004;32(16):4876–83.

[35] Collet JP et al. The elasticity of an individual fibrin fiber in a clot. Proc Natl Acad Sci USA 2005;102(26):9133–7.

[36] Zussman E et al. Mechanical and structural characterization of electrospun PAN-derived carbon nanofibers. Carbon 2005;43(10):2175–85.

[37] Pai C-L, Boyce MC, Rutledge GC. Morphology of porous and wrinkled fibers of polystyrene electrospun from dimethylformamide. Macromolecules 2009;42(6):2102–14.

[38] Lim CT, Tan EPS, Ng SY. Effects of crystalline morphology on the tensile properties of electrospun polymer nanofibers. Appl Phys Lett 2008;92(14):141908.

[39] Chen Z et al. Mechanical properties of electrospun collagen–chitosan complex single fibers and membrane. Mater Sci Eng C 2009;29(8):2428–35.

[40] Matthews JA et al. Electrospinning of collagen nanofibers. Biomacromolecules 2002;3:232–8.

[41] He J-H, Wan Y-Q, Yu J-Y. Effect of concentration on electrospun polyacrylonitrile (PAN) nanofibers. Fibers Polym 2008;9(2):140–2.

[42] Zong-Gang C et al. Diameter control of electrospun chitosan–collagen fibers. J Polym Sci Part B: Polym Phys 2009;47(19):1949–55.

[43] Wenger MPE et al. Mechanical properties of collagen fibrils. Biophys J 2007;93(4):1255–63.

[44] Creighton TE. Proteins: structures and molecular properties. 2nd ed. New York: W.H. Freeman and Co; 1993.

[45] Yang L et al. Mechanical properties of single electrospun collagen type I fibers. Biomaterials 2008;29(8):955–62.

[46] Li M et al. Electrospun protein fibers as matrices for tissue engineering. Biomaterials 2005;26(30):5999–6008.

[47] Guthold M et al. A comparison of the mechanical and structural properties of fibrin fibers with other protein fibers. Cell Biochem Biophys 2007;49(3):165–81.

[48] Agoram B, Barocas VH. Coupled macroscopic and microscopic scale modeling of fibrillar tissues and tissue equivalents. J Biomed Eng 2001;123(4):362–9.

[49] Chandran PL, Barocas VH. Deterministic material-based averaging theory model of collagen gel micromechanics. J Biomech Eng 2007;129:137–47.

[50] Stylianopoulos T, Barocas VH. Volume-averaging theory for the study of the mechanics of collagen networks. Comput Methods Appl Mech Eng 2007;196:2981–90.

[51] Gardel ML et al. Elastic behavior of cross-linked and bundled actin networks. Science 2004;304(5675):1301–5.

[52] Storm C et al. Nonlinear elasticity in biological gels. Nature 2005;435(7039):191–4.

[53] Zeng J et al. Biodegradable electrospun fibers for drug delivery. J Control Release 2003;92(3):227–31.

[54] Im JS et al. Fluorination of electrospun hydrogel fibers for a controlled release drug delivery system. Acta Biomater 2010;6(1):102–9.

[55] Tian M et al. Bis-GMA/TEGDMA dental composites reinforced with electrospun nylon 6 nanocomposite nanofibers containing highly aligned fibrillar silicate single crystals. Polymer (Guildf) 2007;48(9):2720–8.